Received: 20 August 2022 | Revised: 17 September 2022 | Accepted: 9 October 2022

DOI: 10.1002/cey2.299

RESEARCH ARTICLE

CARBON ENERGY WILEY

Atomically bonding Na anodes with metallized ceramic electrolytes by ultrasound welding for high-energy/power solid-state sodium metal batteries

Dongchen Li[1] | Xinxin Wang[1] | Qi Guo[1] | Xiaole Yu[1] | Shangxu Cen[2] | Huirong Ma[2] | Jingjing Chen[2] | Dajian Wang[2] | Zhiyong Mao[1,2] | Chenlong Dong[1,2]

[1]Tianjin Key Laboratory for Photoelectric Materials and Devices, School of Materials Science and Engineering, Tianjin University of Technology, Tianjin, People's Republic of China

[2]Key Laboratory of Display Materials and Photoelectric Devices, Tianjin University of Technology, Ministry of Education, Tianjin, People's Republic of China

Correspondence
Zhiyong Mao and Chenlong Dong, Tianjin Key Laboratory for Photoelectric Materials and Devices, School of Materials Science and Engineering, Tianjin University of Technology, 300384 Tianjin, People's Republic of China.
Email: mzhy1984@163.com and dongchenlong@email.tjut.edu.cn

Funding information
Scientific Developing Foundation of Tianjin Education Commission, Grant/Award Number: 2018ZD09; National Natural Science Foundation of China, Grant/Award Number: 52202282

Abstract

A solid-state sodium metal battery has cut a striking figure in next-generation large-scale energy storage technology on account of high safety, high energy density, and low cost. Nevertheless, the large interfacial resistance and sodium dendrite growth originating from the poor interface contact seriously hinder its practical application. Herein, a modified ultrasound welding was proposed to atomically bond Na anodes and Au-metalized $Na_3Zr_2Si_2PO_{12}$ electrolytes associated with the in situ formation of Na–Au alloy interlayers. Thereupon, intimate $Na_3Zr_2Si_2PO_{12}$–Au/Na interfaces with a low interfacial resistance (~23 Ω cm^2) and a strong dendrite inhibition ability were constructed. The optimized Na symmetric battery can cycle steadily for more than 900 h at 0.3 mA cm^{-2} under a low overpotential (<50 mV) of Na electroplating/stripping and deliver a high critical current density of 0.8 mA cm^{-2} at room temperature. By incorporating the above interface into the solid-state Na metal battery, taking three-dimensional $Na_3V_2(PO_4)_3$ as the cathode, the full battery offers a high energy density of 291 Wh kg^{-1} at a high power density of 1860 W kg^{-1}. A pouch-type solid-state sodium metal full battery based on a ceramic electrolyte was assembled for the first time, and it lit a 3 V LED lamp. Such a strategy of the ultrasound welding metalized solid-state electrolyte/Na interface by engineering the Na–Au interlayer would pave a new pathway to engineer a low-resistance and highly stable interface for high-energy/density solid-state sodium metal batteries.

KEYWORDS

intimate interface contact, metallized ceramics, Na–Au interlayer, solid-state sodium metal battery, ultrasound welding

Dongchen Li and Xinxin Wang contributed equally to this study.

1 | INTRODUCTION

Driven by the increasing demand for large-scale energy storage in power systems, sodium ion batteries are a promising substitute for lithium-ion batteries because of their low cost and rich resources.[1–3] However, the usage of flammable liquid organic electrolytes in sodium ion batteries triggers serious safety issues.[4] Alternatively, solid-state sodium metal batteries manifest high safety and energy density, because the employed solid-state electrolyte is nonflammable and can couple with metal anodes and high-voltage cathodes.[5] NASICON-type (e.g., $Na_3Zr_2Si_2PO_{12}$, donated as NZSP) solid-state electrolytes have wide electrochemical stability window, good thermal stability, and high room-temperature ionic conductivity (10^{-4}–10^{-3} S cm^{-1}).[1,6,7] Despite these, the practical applications of solid-state sodium metal batteries are still hindered by the large interfacial resistance and sodium dendrite growth due to the poor interface contact between NZSP electrolytes and Na anodes.[8–10]

As a matter of fact, the in situ formed interfacial compositions for NZSP/Na interfaces are sodium silicates (e.g. Na_2SiO_3, $Na_2Si_2O_5$).[7,11] Although the sodium silicates are considered Na^+ conductors and used as addition agents in NZSP ceramics during sintering to effectively increase the ionic conductivity resulting from the decreased grain boundary resistance,[12,13] the intrinsic ionic conductivity of sodium silicates (10^{-6} S cm^{-1}) is lower than that of the NZSP (10^{-4} S cm^{-1}).[14] Besides, the uncontrolled reaction between Na and NZSP accompanied by the continuous formation of sodium silicates seriously increases interfacial resistance and decreases critical current density (CCD), resulting in uneven Na dendrite growth and battery failure.[8,15]

To ensure the intimate contact between Na anodes and NZSP electrolytes, the interface of Na/NZSP ought to be modified. Melting and statically pressing (SP) Na on NZSP surfaces appear to be a relatively facile strategy for enhancing interfacial contact by modifying the wettability of Na on NZSP surfaces.[16,17] Nevertheless, high temperature and pressure would accelerate the side reaction of Na and NZSP and go so far as to have the possibility of penetrating the Na metal throughout the NZSP pellet. The interlayer introduction (e.g., MOFs,[15] AlF_3,[18] TiO_2,[19] and Sn/SnO_x[20]), serving as a mechanical buffer matrix, was considered to be an effective way to refine interfacial contact by suppressing dendrite growth and reducing the interfacial resistance. Recently, a room-temperature ultrasound welding method was reported by our group to construct a tightly bonding interface between Na and NZSP electrolytes.[11] However, due to the continuous Na reaction with NZSP electrolytes, the CCD value should endeavor to rise. Worthy of note is that the comprehensive electrochemical performance of solid-state batteries not only is dependent on the interfacial contact of Na anodes and NZSP electrolytes but also strongly relies on the ion/electron transport property and mechanical stability, which are dominantly determined by the interfacial composition.[8] Last but not least, welding between metals and ceramics remains challenging due to physiochemical property differences.[21] Fortunately, the welding of ceramics and metals can be successfully realized by the pretreatment technology of ceramic metallization in the field of semiconductor chips.[22]

Motivated by the ceramic metallization technology, an ~40 nm Au thin layer was vacuum-evaporated on NZSP ceramics (Au-NZSP) and thus enabled the feasibility of atomic bonding between Na anodes and NZSP electrolytes via the ultrasound welding process, accompanied by the formation of the Na–Au alloy interface layer (Figure 1A). Benefitting from the atomic bonding of NZSP-Au and Na metals, the interface resistance can decrease to 23 Ω cm^2 compared with that by the SP method (SP Na/Au-NZSP: 50 Ω cm^2, SP Na/NZSP: 108 Ω cm^2). The Na symmetric battery delivers a high current density of 0.8 mA cm^{-2} at room temperature and it can be stably operated at 0.3 mA cm^{-2} for 900 h with a low overpotential of <50 mV. The solid-state Na-metal full battery harvests a high energy density of 291 Wh kg^{-1} at a high power density of 1860 W kg^{-1}. This work would break new ground in addressing the intractable interface stability of solid-state electrolytes/Na anodes, and thereout, it accelerates the practical application of solid-state sodium metal batteries.

2 | EXPERIMENTAL SECTION

2.1 | Material preparation

NZSP solid electrolytes were synthesized by conventional solid-state sintering. Stoichiometric amounts of Na_2CO_3, ZrO_2, SiO_2, and $NH_4H_2PO_4$ were wet-milled with ethanol (EtOH) for 12 h using a planetary ball mill and then sintered at 1100°C for 12 h. Among them, 15 wt.% excess Na_2CO_3 and $NH_4H_2PO_4$ were added to compensate for the volatilization of Na and P at high temperatures. The precursor was ball-milled, ergo-pressed into green pellets with a diameter of 16 mm, and finally sintered at 1250°C for 6 h in muffle furnace. The thickness of NZSP electrolyte pellets was ~900 μm. The density of the prepared NZSP electrolyte pellets was 3.10–3.13 g cm^{-3} with a relative density of ~95%, according to our previous work.[11]

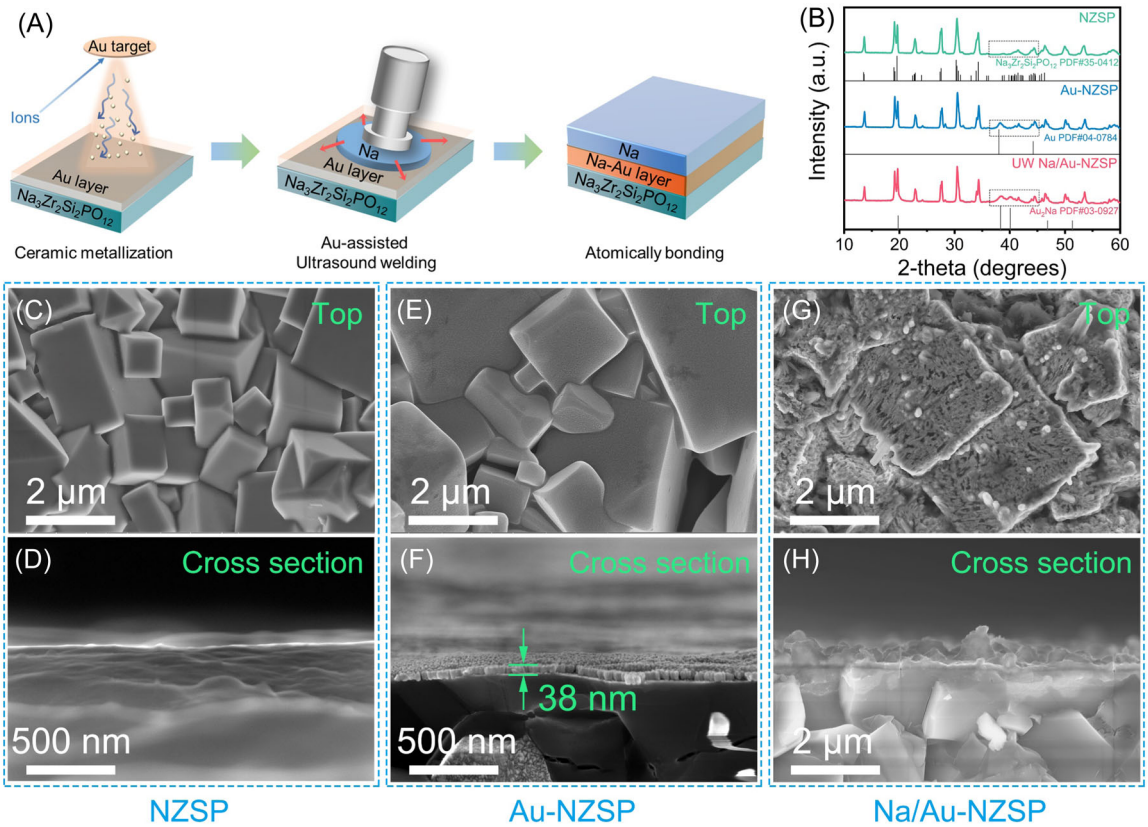

FIGURE 1 (A) Schematic illustration of atomic bonding of Na metal and NZSP pellet by engineering the Na–Au alloy interlayer. (B) XRD patterns of NZSP, Au-NZSP, and UW Na/Au-NZSP. (C) Top-view and (D) cross-section SEM images of the NZSP pellet. (E) Top-view and (F) cross-section SEM images of the Au-NZSP pellet. (G) Top-view and (H) cross-section SEM images of the UW Na/Au-NZSP pellet. SEM, scanning electron microscopy; XRD, X-ray diffraction.

2.2 | Atomically bonding Na metals with NZSP

The adhesive layer should possess good sodiophilicity and low overpotential of Na deposition. According to the binary phase diagram of Na-M, Au, Ag, In, Ge, Sn, Sb, and Bi can be able to form thermodynamically stable alloys with Na metals. However, Mo, Cr, Fe, Co, Cu, and others cannot alloy with Na. The choice of Au as a modification layer is due to its lowest Na nucleation overpotential (~0 V), which is much lower than those of Sn (<5 mV), Sb (<5 mV), Cu (16 mV), Cr (19 mV), and Mo (21 mV).[23] The Au layer coating on the NZSP electrolyte surface was prepared by ion sputtering deposition. The deposition was performed in a sputter coater (KYKYSBC-12) and pre-evacuated at 8–10 Pa with a discharge current of 10 mA for 200 s without inflation of extra gas at room temperature. The NZSP surface was located at a distance of 35 mm from the gold target (99.99% in purity). The household ultrasonic cleaner (JEKEN CE-9600, power = 70 W, frequency = 50 kHz) was employed to construct Na–Au alloy interlayers between Na metal anodes and NZSP electrolytes as previously reported by our group.[11] During ultrasound welding, there is no additional force perpendicular to the NZSP plane except for the static pressure generated by the gravity of the ultrasound probe. For comparison, the Na/Au-NZSP and Na/NZSP interfaces were prepared by the static pressing method (Kejing MSK-160E) with a pressure of ~9.4 MPa.

2.3 | Preparation of large-area NZSP films

The mashed NZSP powder was suspended in EtOH and triethanolamine (TEA) solution and ball-milled for 30 min at 1200 rpm. Then, the dibutyl phthalate (DBP) and dioctyl phthalate (DOP) as the plasticizer and polyvinyl butyral (PVB) as the binder were added into the above mixture and further ball-milled for 1 h at 1200 rpm. The mass ratio of NZSP:EtOH:TEA:DBP:-DOP:PVB is 52:37:1:2.5:2.5:5. The ball-milled slurry was transfered into a vacumm oven to remove the bubble at room temperature. The slurry was tape-casted on a release liner (fluorinated ethylene propylene) to obain

a NZSP film precursor and dried in a vacuum oven at 60°C for 12 h. The dried NZSP film precursor was peeled off and cut into a 6 cm × 3.5 cm film. Finally, the NZSP film precursor was first annealed at 600°C for 2 h to remove the binder/plasticizer/dispersant and finally sintered at 1200°C for 12 h for densification of the NZSP film (heating rate: 1°C min^{-1}).

2.4 | Characterizations

X-ray diffraction (XRD) (ARL Equinox 3000) was operated at 40 kV and 40 mA with a 2θ range of 10−80° to examine the crystal phase of prepared samples. The microstructure and elemental composition were recorded on a field-emission scanning electron microscope (SEM) (FEI-Quanta FEG) and ultrahigh-resolution field-emission SEM (FEI-Verios 460L). The NZSP pellet, Au-NZSP pellet, and UW Na/Au-NZSP pellet for SEM tests were not polished by emery paper. For the UW Na/Au-NZSP pellet, it was stored in a glovebox to avoid the exposure to air and put into a sealed bottle until the SEM test. However, this UW Na/Au-NZSP pellet should be taken from the bottle and then transferred into a vacuum system of SEM. Therefore, the transient exposure into air is difficult to avoid.

2.5 | Electrochemical measurements

Electrochemical impedance spectroscopy (EIS) measurements of the electrolyte were tested on an electrochemical workstation (CHI760E) under an open-circuit potential with an amplitude of 5 mV and frequency ranging from 100 kHz to 0.01 Hz. A thin layer of Au was sputtered on each surface of the pellets as blocking electrodes. The Na symmetric batteries were assembled into a CR2032 coin cell to investigate the performance of long-term cycling and CCD in an argon-filled glove box at room temperature. Critical current measurements were performed by the galvanostatic cycling at current densities stepping from 0.05 to 1.5 mA cm^{-2} (step length: 0.05 mA cm^{-2}, electroplating/stripping time: 0.5 h) at room temperature. The CR2032 full battery was assembled using sodium foil as the anode, NZSP pellet as the electrolyte, and NVP as the cathode material in an argon-filled glovebox at room temperature. Commercial NVP (Hubei Energy Technology Co., Ltd.), acetylene black, and poly(vinyldifluoride) (PVDF) with a weight ratio of 8:1:1 were mixed in *N*-methyl pyrolidone to form a homogeneous slurry, ergo-coated on aluminum foil by a doctor blade, and finally dried at 120°C for 24 h in a vacuum oven. The mass loading of NVP was ~1 mg cm^{-2}. The liquid electrolyte (10 μL) (1 M $NaClO_4$ in EC/DMC (1:1) + 5% FEC) was added between the cathode and electrolyte pellet to establish a wetted interface.

3 | RESULTS AND DISCUSSION

The NZSP solid-state electrolyte was initially prepared by the high-temperature solid-state method. The XRD pattern (Figure 1B) suggests that the NZSP crystallizes into monoclinal $Na_3Zr_2Si_2PO_{12}$ with space group of $C2/c$ ($a = 15.637$ Å, $b = 9.023$ Å, $c = 9.217$ Å, $\alpha = \gamma = 90°$, $\beta = 123.75°$). Then, the NZSP ceramic pellet was metalized by an ultrathin Au layer via vacuum ion sputtering, as illustrated in Figure 1A. The new peaks at 38.2° and 44.4° in the XRD pattern of Au-NZSP can be indexed into cubic Au ($Fm\bar{3}m$, $a = b = c = 4.079$ Å, $\alpha = \beta = \gamma = 90°$), providing the presence of the Au coating layer on the surface of the electrolyte. After the Au deposition, the surface color of the NZSP pellet changes from white to brick red (digital image: Figure S1). Finally, the sodium metal anode was placed on the surface of Au/NZSP and thereupon ultrasound-welded, which resulted in the formation of cubic Au_2Na ($Fd\bar{3}m$, $a = b = c = 7.812$ Å, $\alpha = \beta = \gamma = 90°$),[24,25] and the resultant interface color changes into deep red (Figure 1B and Figure S1). The above results articulated that Na and Au reacted to form the Au–Na alloy under room-temperature ultrasound welding.

The top-view SEM image of the sintered NZSP pellet suggests the micron-scale cube morphology of crystal grains (Figure 1C) and the corresponding cross-section image confirms the relatively compact structure inside the NZSP pellet (Figure 1D). After coating the Au layer, the smooth NZSP grains were covered by gold nanoparticles, generating a relatively rough surface (Figure 1E). As expected, the ion-sputtered Au nanoparticles can cover the surface of NZSP grains and grain boundaries evenly (Figures S2 and S3). The cross-section SEM image of Au/NZSP provides conspicuous evidence that the ultrathin Au layer with ~38 nm thickness was successfully deposited on the NSZP surface with neatly arranged Au nanoparticles (Figure 1F). After ultrasound welding of Na metals on Au/NZSP, the unique mossy morphology can be observed (Figure 1G and Figure S4), which proves that the Na metal reacts with Au to form Na–Au nanoparticles on the surface of the NZSP micron-scale cube. The cross-section SEM image of Na/Au-NZSP (Figure 1H) indicates that the Au–Na interlayer with rough and concave–convex morphology is tightly bonded on the surface of the NZSP pellet and the interface between Na and Au-NZSP is consecutive without any pores and defects.

To further comprehend the effects of interface composition and contact property on interface stability, the interfacial microstructures of the SP Na/NZSP interface (donated as SP Na/NZSP), UW Na/NZSP interface, and UW Na/Au-NZSP have been surveyed, as modeled as Figure 2A. The cross-section SEM image of the SP Na/NZSP interface (Figure 2B) manifests the huge gap and poor contact, which would cause huge interface resistance, failure of Na^+ transport, and uneven Na electroplating/stripping.[26] Nevertheless, for the UW Na/NZSP interface, although an intimate and dense interface layer can be observed (Figure 2C), the low ionic conductivity of the interfacial Na_2SiO_3 interlayer would induce inhomogeneous Na^+ transport.[15,27] Moreover, due to the absence of the protective layer between Na and NZSP, the highly spontaneous reactivity gradually decreases the proportion of the highly ion-conductive NZSP solid-state electrolyte. Instead, a continuous, dense, and flat Na/Au-NZSP interface is engineered by ultrasound welding (Figure 2D), in which the Na–Au interlayer can protect from the direct contact between highly active Na metals and NZSP electrolytes, thereby ensuring the rapid Na^+ transport. Moreover, the grain boundaries and voids on the surface of ceramic electrolyte pellets are unavoidable even after grinding and polishing, which may become a destination for local Na deposition.[28–31] It is reassuring that the Au–Na alloy formed by ultrasonic welding can fully fill the above defects and inhibit the growth of dendrites. The EDX elemental mappings of the cross-section of the UW Na/Au-NZSP pellet are revealed in Figure S5, in which the continuous distribution of Na signals proved that the interface was closely contacted. To further visualize the adhesive ability of Na on NZSP pellets, the Na was tried to scrape off from the NZSP surface by a knife, as shown in Figure S6. Conspicuously, at the UW Na/Au-NZSP interface, the Na metal was difficult to be removed after vigorous scraping, indicating the intimate contact between Na and the

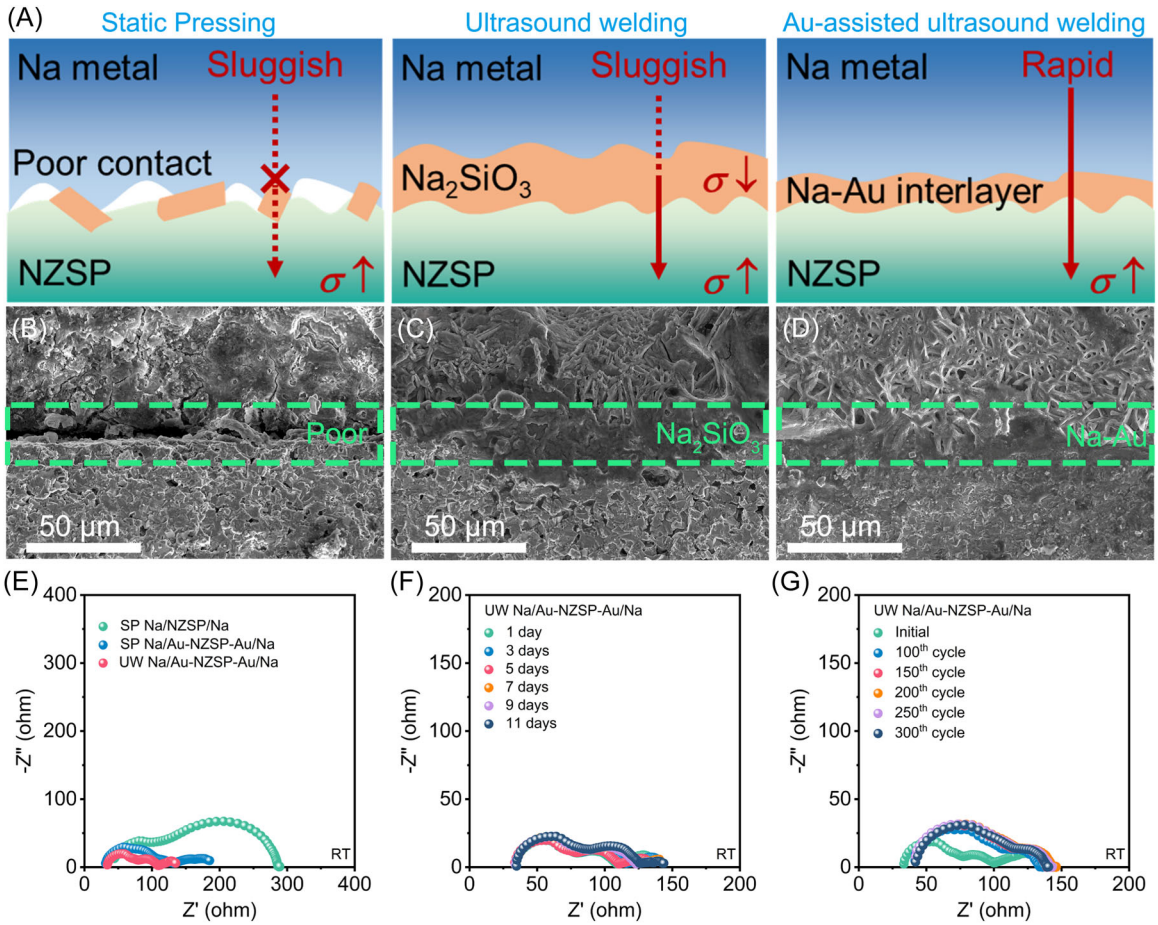

FIGURE 2 (A) Schematic models of SP Na/NZSP, UW Na/NZSP, and UW Na/Au-NZSP interfaces. Cross-section SEM images of the (B) SP Na/NZSP, (C) UW Na/NZSP, and (D) UW Na/Au-NZSP interfaces. (E) EIS data of the assembled SP Na/NZSP/Na, SP Na/Au-NZSP-Au/Na battery, and UW Na/Au-NZSP-Au/Na symmetrical battery. (F) EIS evolution of the UW Na/Au-NZSP-Au/Na symmetrical battery during 11 days. (G) EIS data of the UW Na/Au-NZSP-Au/Na symmetrical battery measured at 0.1 mA cm^{-2} after certain cycles. EIS, electrochemical impedance spectroscopy; SEM, scanning electron microscopy; SP, statically press.

Au-$Na_3Zr_2Si_2PO_{12}$ pellet (Figure S6A). While for UW Na/NZSP (Figure S6B), SP Na/Au-NZSP (Figure S6C), and SP Na/NZSP (Figure S6D), relatively large areas of sodium can be removed, especially for SP Na/NZSP. Therefore, the aid of the intimate Na/NZSP interface has been realized by ultrasound welding-assisted ceramic metallization.

The Nyquist plots of the NZSP pellet suggest a total resistance of ~95 Ω (Figure S7), corresponding to the ionic conductivity of 4.5×10^{-4} S cm^{-1} at room temperature. To investigate the interface composition and contact property on interface character, the SP Na/NZSP/Na, SP Na/Au-NZSP-Au/Na, and UW Na/Au-NZSP-Au/Na symmetrical batteries were assembled. As shown in Figure 2E, for SP Na/NZSP/Na and SP Na/Au-NZSP-Au/Na, the starting point of the Nyquist plots corresponds to the bulk resistance of the NZSP pellet, and the first and second semicircle represent the grain boundary resistance of the electrolyte and the interface resistance of Na/NZSP, respectively.[32] In an ideal situation, the charge transfer across two Na/NZSP interfaces should be identical in a symmetric battery. For the SP Na/NZSP/Na symmetrical battery, the overall resistance was ~290 Ω, and the interface resistance of Na/NZSP was calculated to be ~108 Ω cm^2. The total resistance of the UW Na/Au-NZSP-Au/Na battery was ~135 Ω, in which the Nyqusit plot was composed of three semicircles and the middle semicircle represents the interface impedance of the NZSP pellet and Na–Au alloy interlayer. The UW Na/Au-NZSP shows a lower interface resistance of ~23 Ω cm^2 than SP Na/Au-NZSP (~50 Ω cm^2). Additionally, the almost unchanged resistance value of UW Na/Au-NZSP-Au/Na within 11 days further proves the stability of the Na–Au alloy interlayer (Figure 2F).

Galvanostatic CCD, as a significant evolution indicator, was performed to evaluate the Na electroplating/stripping ability with gradually increasing current density (Figure 3A–C).[33–35] The CCD of the UW Na/Au-NZSP-Au/Na symmetrical battery can reach 0.8 mA cm^{-2} at room temperature, which is higher than those of SP Na/NZSP/Na (0.3 mA cm^{-2}), SP Na/Au-NZSP-Au/Na (0.5 mA cm^{-2}), and previously reported UW Na/NZSP/Na (0.6 mA cm^{-2}).[11] Such CCD results confirm that the Na–Au alloy interlayer effectively ensures the uniform Na^+ transport. Galvanostatic charge/discharging of Na

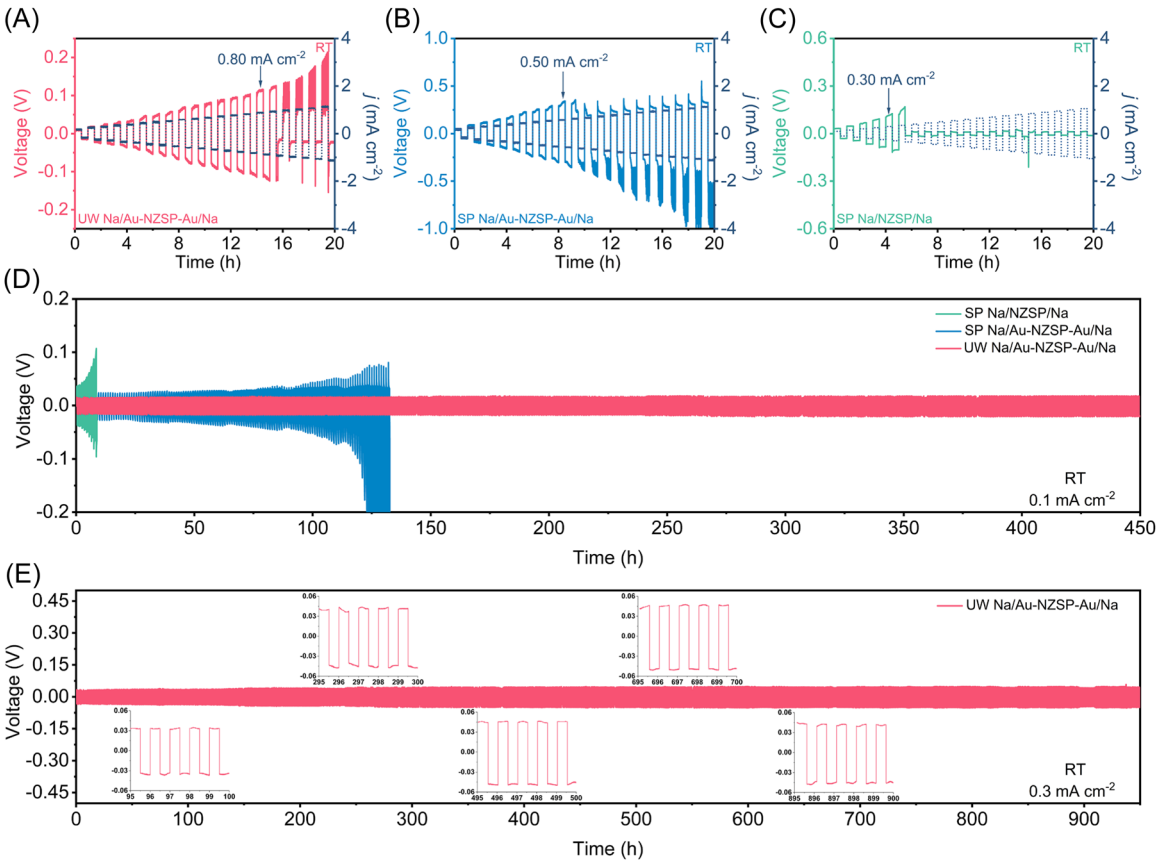

FIGURE 3 Critical current density of (A) UW Na/Au-NZSP-Au/Na, (B) SP Na/Au-NZSP-Au/Na, and (C) SP Na/NZSP/Na symmetrical batteries at room temperature. (D) Galvanostatic charging/discharging curves of the UW Na/Au-NZSP-Au/Na symmetrical battery at a current density of 0.1 mA cm^{-2} at room temperature. (E) Galvanostatic cycling curves of the UW Na/Au-NZSP-Au/Na symmetrical battery at a current density of 0.3 mA cm^{-2} at room temperature.

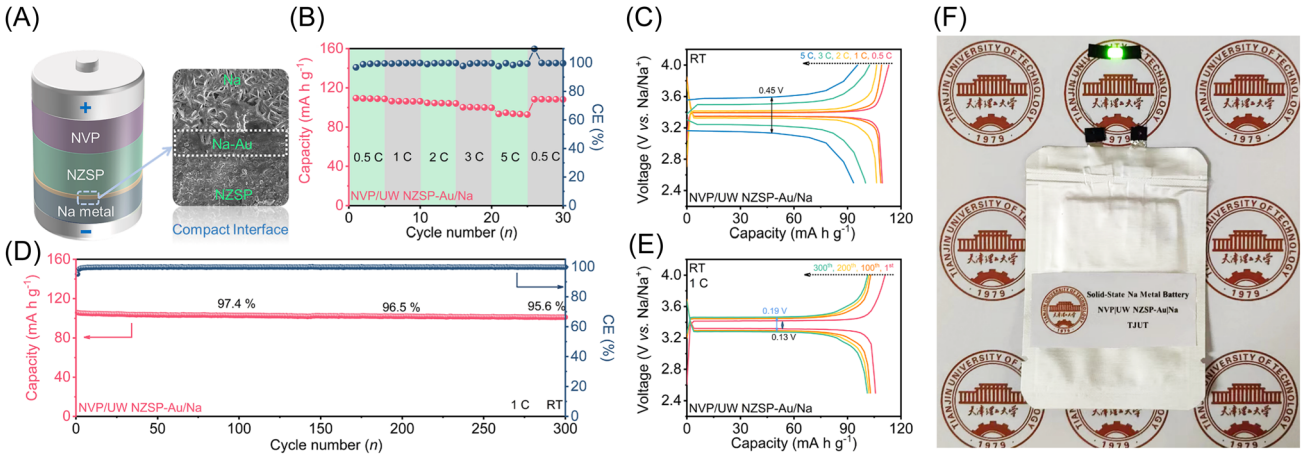

FIGURE 4 (A) Schematic illustration of the assembled NVP|UW NZSP-Au|Na sodium metal full battery. (B) Rate performance and (C) corresponding charging/discharging profiles of the NVP|UW NZSP-Au|Na battery. (D) Cycling performance and (E) corresponding galvanostatic charging/discharging curves of the NVP|UW NZSP-Au|Na battery at 1 C at room temperature. (F) Digital micrograph of a single-chip pouch cell (NVP|UW NZSP-Au|Na).

symmetric batteries was carried out to further estimate the interfacial stability. The UW Na/Au-NZSP-Au/Na symmetrical battery can stably be cycled for 450 h at 0.1 mA cm^{-2} with a Na electroplating/stripping overpotential of ~18 mV (Figure 3D). While for the SP Na/NZSP/Na and SP Na/Au-NZSP-Au/Na, the symmetrical batteries fail in 10 and 130 h, respectively. Meanwhile, the resistance value of the UW Na/Au-NZSP-Au/Na symmetrical battery in 300 h retains as the initial level (Figure 2G). Meanwhile, the shapes of Nyquist plots get changed after 100 h, where the boundaries between semicircles became blurred. This phenomenon is attributed to alloying/dealloying transformation during Na electroplating/stripping.[36] Even at the current density of 0.3 mA cm^{-2}, the UW Na/Au-NZSP-Au/Na symmetrical battery can steadily operate for 900 h and maintain a low overpotential of <45 mV at room temperature (Figure 3E).

To comprehend the stability of the Na–Au alloy interlayer after long-term cycling at 0.3 mA cm^{-2}, the UW Na/Au-NZSP-Au/Na battery was disassembled, and the NZSP pellet was characterized on SEM after removing the Na anode by EtOH (Figure S8). Obviously, there are still abundant mossy Na–Au alloys on the surface of the NZSP pellet, which were tightly attached to the NZSP grains and filled in grain boundaries. The NZSP grains maintain initial micron-scale cube morphology, indicating that the reaction between the Au layer and Na anode induced by ultrasonic welding as well as the charge/discharge process had no microstructural effect on the NZSP electrolyte. Besides, the XRD has been performed to investigate the composition of UW Na/Au-NZSP before and after cycling, as shown in Figure S9. Compared with initial UW Na/Au-NZSP, there is no obvious change for the XRD pattern of UW Na/Au-NZSP after cycling and the expected Na_2Au phase can be also detected. The origin of remarkable electrochemical performance of the UW Na/Au-NZSP-Au/Na symmetrical battery can be concluded as follows. The Au interlayer between the NZSP electrolyte pellet and Na metal anode can provide compact contact, which is realized by introducing the Na–Au interlayer via ultrasound welding solid-state electrolytes and Na anodes. The Au layer on NZSP tables can enhance the wettability of Na on the NZSP surface by the formation of Na–Au alloys. Such Na–Au alloy interlayers ensure the rapid Na^+ transport and low overpotential of Na electroplating/stripping.

To put the highly stable UW Na/Au-NZSP interface into practice, taking three-dimensional $Na_3V_2(PO_4)_3$ (NVP) with the opened Na^+ transport channel as the cathode, the NVP|UW NZSP-Au|Na solid-state sodium metal full battery was assembled, as illustrated in Figure 4A. The theoretical capacity of $Na_3V_2(PO_4)_3$ is 118 mA h g^{-1} based on the redox pair of V^{4+}/V^{3+} (1 C = 118 mA g^{-1}). The NVP|UW NZSP-Au|Na can offer capacities of 109.5 mA h g^{-1} at 0.5 C, 106.4 mA h g^{-1} at 1 C, 104.7 mA h g^{-1} at 2 C, 100.3 mA h g^{-1} at 3 C, and 93.4 mA h g^{-1} at 5 C (Figure 4B). Especially at the rate of 5 C, the full battery can offer a high energy density of 291 Wh kg^{-1} at a high power density of 1860 W kg^{-1}, which is among the best in NZSP-based sodium metal batteries (Table S1). Reassuring that, when the current density is reset to 0.5 C, the discharge capacity can recover into the initial level (108.3 mA h g^{-1}). The voltage difference of charging/discharging plateaus for the NVP|

UW NZSP-Au|Na battery is only 0.45 V at 5 C, further suggesting the rapid Na^+ transport and stably compact interfacial contact (Figure 4C).

The NVP|UW NZSP-Au|Na battery offers an initial discharge capacity of 105.7 mA h g^{-1} at 1 C with an initial Coulombic efficiency of 95.2 (Figure 4D). After 300 cycles, it harvests a specific capacity of 101.1 mA h g^{-1}, corresponding to the high capacity retention of 95.6%. The galvanostatic charging/discharging profiles (Figure 4E) of the NVP|UW NZSP-Au|Na battery were performed within the potential window of 2.5–4 V. The discharging plateau at ~3.3 V and charging plateau at ~3.4 V are contributed by the reversible redox reaction of V^{3+}/V^{4+}.[37,38] The voltage difference of charging/discharging plateaus is 0.13 V in the first cycle and lagged by only 60 mV after 300 cycles. Besides, the highly overlapped charge/discharge profile of the NVP|UW NZSP-Au|Na battery at 1 C within 300 cycles implies the superior cycling stability. To verify the feasibility of ultrasound welding Na anodes with metallized ceramic electrolytes in large-scale applications for high-energy/power solid-state sodium metal batteries, a single-chip pouch cell (NVP|UW NZSP-Au|Na) was assembled with a plane size of 3.5 cm × 4.5 cm by using a 700-μm-thickness NZSP pellet (Figure 4F and Figure S10). Such a pouch cell can light a 3 V LED lamp, which further proves its potential for practical application.

4 | CONCLUSION

In summary, the atomically bonded Na–Au alloy interlayer is engineered by ultrasound welding Na with the Au/NZSP pellet. The Na–Au alloy interlayer can avoid the excess formation of the Na_2SiO_3 byproduct, accelerate the Na^+ transport, and promote the uniform Na electroplating/stripping. Benefitting from the merits of the compact Na/Au-NZSP interface, the interface resistance can decrease to 23 Ω cm^2. The Na/Au-NZSP-Au/Ns symmetrical battery can provide a high CCD of 0.8 mA cm^{-2} and stably cycle at 0.3 mA cm^{-2} for 900 h with a low overpotential of 45 mV. When served as a sodium metal full battery, the assembled NVP|UW NZSP-Au|Na battery can offer a high-energy density of 291 Wh kg^{-1} at a high-power density of 1860 W kg^{-1}. The NVP|UW NZSP-Au|Na battery retains a high capacity retention of 95.6% at 1 C after 300 cycles. The atomically suturing Na metal and metallized oxide ceramics would guide the rational design of the stable and compact Na/electrolyte interface, thus accelerating the development of high-power-density and high-energy-density solid-state sodium metal batteries.

ACKNOWLEDGMENTS

This work was supported by the National Natural Science Foundation of China (Grant Nos. 51777138, 52202282) and Scientific Developing Foundation of Tianjin Education Commission (Grant No. 2018ZD09).

CONFLICTS OF INTEREST

The authors declare no conflicts of interest.

ORCID

Zhiyong Mao http://orcid.org/0000-0003-0125-3408

REFERENCES

1. Lu Y, Li L, Zhang Q, Niu Z, Chen J. Electrolyte and interface engineering for solid-state sodium batteries. *Joule*. 2018;2(9):1747-1770.
2. Hirsh HS, Li Y, Tan DHS, Zhang M, Zhao E, Meng YS. Sodium-ion batteries paving the way for grid energy storage. *Adv Energy Mater*. 2020;10(32):2001274.
3. Li M, Lu J, Chen Z, Amine K. 30 years of lithium-ion batteries. *Adv Mater*. 2018;30(33):1800561.
4. Huang Y, Zhao L, Li L, Xie M, Wu F, Chen R. Electrolytes and electrolyte/electrode interfaces in sodium-ion batteries: from scientific research to practical application. *Adv Mater*. 2019;31(21):1808393.
5. Janek J, Zeier WG. A solid future for battery development. *Nat Energy*. 2016;1(9):16141.
6. Jian Z, Hu Y-S, Ji X, Chen W. NASICON-structured materials for energy storage. *Adv Mater*. 2017;29(20):1601925.
7. Yang Z, Tang B, Xie Z, Zhou Z. NASICON-type $Na_3Zr_2Si_2PO_{12}$ solid-state electrolytes for sodium batteries. *ChemElectroChem*. 2021;8(6):1035-1047.
8. Bao C, Wang B, Liu P, et al. Solid electrolyte interphases on sodium metal anodes. *Adv Funct Mater*. 2020;30(52):2004891.
9. Matios E, Wang H, Wang C, Li W. Enabling safe sodium metal batteries by solid electrolyte interphase engineering: a review. *Ind Eng Chem Res*. 2019;58(23):9758-9780.
10. Li Z, Liu P, Zhu K, et al. Solid-state electrolytes for sodium metal batteries. *Energy Fuel*. 2021;35(11):9063-9079.
11. Wang X, Chen J, Wang D, Mao Z. Improving the alkali metal electrode/inorganic solid electrolyte contact via room-temperature ultrasound solid welding. *Nat Commun*. 2021;12:7109.
12. Oh J, He L, Plewa A, et al. Composite NASICON ($Na_3Zr_2Si_2PO_{12}$) solid-state electrolyte with enhanced Na^+ ionic conductivity: effect of liquid phase sintering. *ACS Appl Mater Interfaces*. 2019;11(43):40125-40133.
13. Santhoshkumar B, Choudhary MB, Bera AK, Yusuf SM, Ghosh M, Pahari B. High Na^+ conducting $Na_3Zr_2Si_2PO_{12}$/$Na_2Si_2O_5$ composites as solid electrolytes for Na^+ batteries. *J Am Chem Soc*. 2022;105(7):5011-5019.
14. Chatterjee S, Saha SK, Chakravorty D. Ionic conductivity of sodium silicate glasses grown within confined volume of mesoporous silica template. *AIP Conf Proc*. 2018;1942(1):140027.
15. Miao X, Wang P, Sun R, et al. Liquid metal-organic frameworks in-situ derived interlayer for high-performance solid-

state Na-metal batteries. *Adv Energy Mater*. 2021;11(47):2102396.
16. Uchida Y, Hasegawa G, Shima K, et al. Insights into sodium ion transfer at the Na/NASICON interface improved by uniaxial compression. *ACS Appl Energy Mater*. 2019;2(4):2913-2920.
17. Zhou W, Li Y, Xin S, Goodenough JB. Rechargeable sodium all-solid-state battery. *ACS Cent Sci*. 2017;3(1):52-57.
18. Miao X, Di H, Ge X, et al. AlF_3-modified anode-electrolyte interface for effective Na dendrites restriction in NASICON-based solid-state electrolyte. *Energy Storage Mater*. 2020;30:170-178.
19. Gao Z, Yang J, Li G, et al. TiO_2 as second phase in $Na_3Zr_2Si_2PO_{12}$ to suppress dendrite growth in sodium metal solid-state batteries. *Adv Energy Mater*. 2022;12(9):2103607.
20. Yang J, Xu H, Wu J, et al. Improving Na/$Na_3Zr_2Si_2PO_{12}$ interface via SnO_x/Sn film for high-performance solid-state sodium metal batteries. *Small Methods*. 2021;5(9):2100339.
21. Zhang Y, Chen Y, Yu D, Sun D, Li H. A review paper on effect of the welding process of ceramics and metals. *J Mater Res Technol*. 2020;9(6):16214-16236.
22. Yang X, Xiong X, Jin W, Zhao G, Peng Z, Cao F. Research progress of ceramic metallization technology. *Res Appl Mater Sci*. 2020;2(1):12-16.
23. Tang S, Zhang YY, Zhang X-G, et al. Stable Na plating and stripping electrochemistry promoted by in situ construction of an alloy-based sodiophilic interphase. *Adv Mater*. 2019;31(16):1807495.
24. Qiao H, Nohira T, Ito Y. Electrochemical formation of Au_2Na alloy and the characteristics of (Au_2Na+Au) reference electrode in a LiF–NaF–KF eutectic melt. *Electrochim Acta*. 2002;47(28):4543-4549.
25. Ahsan M, Ali Z, Ysman M, Hou Y. Unfolding the structural features of NASICON materials for sodium-ion full cells. *Carbon Energy*. 2022;4(5):776-819.
26. Wang H, Matios E, Luo J, Li W. Combining theories and experiments to understand the sodium nucleation behavior towards safe sodium metal batteries. *Chem Soc Rev*. 2020;49(12):3783-3805.
27. Sun Z, Zhao Y, Ni Q, et al. Solid-state Na metal batteries with superior cycling stability enabled by ferroelectric enhanced Na/$Na_3Zr_2Si_2PO_{12}$ interface. *Small*. 2022;18(16):2200716.
28. Yu S, Siegel DJ. Grain boundary contributions to Li-ion transport in the solid electrolyte $Li_7La_3Zr_2O_{12}$ (LLZO). *Chem Mater*. 2017;29(22):9639-9647.
29. Raj R, Wolfenstine J. Current limit diagrams for dendrite formation in solid-state electrolytes for Li-ion batteries. *J Power Sources*. 2017;343:119-126.
30. Ren Y, Shen Y, Lin Y, Nan C-W. Direct observation of lithium dendrites inside garnet-type lithium-ion solid electrolyte. *Electrochem Commun*. 2015;57:27-30.
31. Wang S, Xu H, Li W, Dolocan A, Manthiram A. Interfacial chemistry in solid-state batteries: formation of interphase and its consequences. *J Am Chem Soc*. 2018;140(1):250-257.
32. Noguchi Y, Kobayashi E, Plashnitsa LS, Okada S. Yamaki J-I. Fabrication and performances of all solid-state symmetric sodium battery based on NASICON-related compounds. *Electrochim Acta*. 2013;101:59-65.
33. Lu Y, Zhao C-Z, Yuan H, Cheng X-B, Huang J-Q, Zhang Q. Critical current density in solid-state lithium metal batteries: mechanism, influences, and strategies. *Adv Funct Mater*. 2021;31(18):2009925.
34. Wang J, Yuan J, Fu Q, et al. Dendrite-free lithium and sodium metal anodes with deep plating/stripping properties for lithium and sodium batteries. *Carbon energy*. 2021;3(1):153-166.
35. Sarkar S, Thangadurai V. Critical current densities for high-performance all-solid-state Li-metal batteries: fundamentals, mechanisms, interfaces, materials, and applications. *ACS Energy Lett*. 2022;7(4):1492-1527.
36. Tang S, Qiu Z, Wang X-Y, et al. A room-temperature sodium metal anode enabled by a sodiophilic layer. *Nano Energy*. 2018;48:101-106.
37. Saravanan K, Mason CW, Rudola A, Wong KH, Balaya P. The first report on excellent cycling stability and superior rate capability of $Na_3V_2(PO_4)_3$ for sodium ion batteries. *Adv Energy Mater*. 2013;3(4):444-450.
38. Zheng Q, Yi H, Li X, Zhang H. Progress and prospect for NASICON-type $Na_3V_2(PO_4)_3$ for electrochemical energy storage. *J Energy Chem*. 2018;27(6):1597-1617.

SUPPORTING INFORMATION

Additional supporting information can be found online in the Supporting Information section at the end of this article.

How to cite this article: Li D, Wang X, Guo Q, et al. Atomically bonding Na anodes with metallized ceramic electrolytes by ultrasound welding for high-energy/power solid-state sodium metal batteries. *Carbon Energy*. 2022;1-9. doi:10.1002/cey2.299